Global Average Gray and White Matter *N*-acetylaspartate Concentration in the Human Brain

Matilde Inglese, **Henry Rusinek**, **Ilena C. George**, **James S. Babb**, **Robert I. Grossman**, and **Oded Gonen**
Department of Radiology, New York University School of Medicine, 650 First Avenue, New York, NY 10016

Abstract

Since the amino acid derivative *N*-acetylaspartate (NAA) is almost exclusive to neuronal cells in the adult mammalian brain and its concentration has shown local (or global) abnormalities in most focal (or diffuse) neurological diseases, it is considered a specific neuronal marker. Yet despite its biological and clinical prominence, the relative NAA concentration in the gray and white matter (GM, WM) remains controversial, with each reported to be higher than, equal to, or less than the other. To help resolve the controversy *and* importantly, access the NAA in both compartments in their entirety, we introduce a new approach to distinguish and quantify the whole-brain average GM and WM NAA concentration by integrating MR-image segmentation, localized and non-localized quantitative ^{1}H-MRS. We demonstrate and validate the method in ten healthy volunteers (5 women) 27±6 years old (mean ± standard-deviation) at 1.5 T. The results show that the healthy adult human brain comprises significantly less WM, 39±3%, than GM 60±4% by volume (*p*<0.01). Furthermore, the *average* NAA concentration, in the WM, 9.5±1.0 mM, is significantly lower than in GM, 14.3 ±1.1 mM (*p*<0.01) with no gender differences (*p*>0.5).

Keywords

Absolute quantification; Brain; gray matter; *N*-acetylaspartate (NAA); proton magnetic resonance spectroscopy (^{1}H-MRS); white matter

Introduction

The amino acid derivative *N*-acetylaspartate (NAA, see Fig. 1) was first described over fifty years ago (Tallan et al., 1956). At up to 0.1% of the brain tissue wet weight, NAA is the second most abundant amino acid in the human central nervous system (CNS) after glutamate (Baslow, 2003). The singlet resonance of the protons of its *N*-acetyl group is the most prominent peak in the proton MR spectrum (^{1}H-MRS) of the brain, as shown in Fig. 1, making it straightforward to quantify non-invasively *in vivo* (Jansen et al., 2006). Since in the mature adult brain NAA is almost exclusively localized in neurons and their processes (Baslow, 2003;Simmons et al., 1991) and although its exact role(s) there are still unknown (Moffett et al., 2007), it is widely considered a putative marker of their density, integrity and viability (Arnold et al., 2001).

Correspondence and Reprint Requests: Oded Gonen, Department of Radiology, New York University School of Medicine, 650 First Avenue, 6th Floor, New York, NY 10016, Tel./FAX (212) 263-3532; (212) 263-7541, e-mail: oded.gonen@med.nyu.edu.

Indeed, among the resonances identified in neuro-^{1}H-MRS, none has yielded more diagnostic information than the NAA. Its regional (or global) concentration decline has been shown in most focal (or diffuse) CNS disorders (Ross and Bluml, 2001; Schuff et al., 2006). To better identify and quantify *diffuse* abnormalities, however, the global NAA concentration must be known in the various compartments of the *healthy* CNS (Jansen et al., 2006), which to a first approximation comprises gray and white matter and cerebrospinal fluid (GM, WM, CSF) (Clark et al., 2006; Pfefferbaum et al., 1999b).

Despite its incontrovertible prominence, however, the NAA concentration of either compartment of the healthy brain remains controversial. For example, a partial sample of the literature shows NAA levels to be 1.2 – 1.5 times *higher* in GM by some (Doyle et al., 1995; Lim and Spielman, 1997; McLean and Barker, 2006; Narayana et al., 1989; Noworolski et al., 1999; Wang and Li, 1998). In contrast, others report the NAA concentration to be more than 1.1 fold *lower* in GM than in WM (Gideon et al., 1995; Hetherington et al., 1996; Schuff et al., 2001; Soher et al., 1996; Tedeschi et al., 1995), while others find it to not differ significantly between the two compartments (Kreis et al., 1993; Lopez-Villegas et al., 1996; Michaelis et al., 1993).

The discrepancy may be due (at least in part) to a confluence of three problem areas: First, neither single-voxel nor two or even three-dimensional (3D) ^{1}H-MRS presently cover the entire brain. Second, the sensitivity of ^{1}H-MRS is insufficient to fully resolve GM from WM. Finally, most cortical GM is difficult to access since it is only 1 – 4 mm thick, tortuous and adjacent to bone marrow and subcutaneous lipids whose signals may obscure the NAA's (Moonen et al., 1992). Consequently, the volume-of-interest (VOI) must often be away from the skull and even careful placement cannot eliminate partial GM/WM volume effects. Although some ^{1}H-MRS studies applied sophisticated tissue segmentation to account for it, they neither eliminated it nor covered the whole brain (Stadlbauer et al., 2004; Weber-Fahr et al., 2002). These issues combine to make the assessment of the total loads of the neuronal and axonal dysfunctions (in the GM and WM) of diffuse neurological disorders inaccessible to the current ^{1}H-MRS methodologies.

To address the above issues, the goal of this paper is to introduce a new method that integrates MRI segmentation, non-localizing whole brain NAA (WBNAA) and 3D ^{1}H-MRS quantification. to distinguish and quantify the *average* global NAA concentrations in the entire GM and WM moieties of healthy volunteers. The rationale for such cohort is that absent a gold standard then for purposes of validation, the precision must be established. Specifically, a reliable method should yield the same WM and GM NAA concentration across all healthy individuals.

Theory

As indicated above, lipid signal contamination renders ^{1}H-MRS unreliable near the skull (Moonen et al., 1992). Although the WBNAA method was developed specifically to overcome this problem, it does so at the expense of localization (Gonen et al., 1998b), yielding the total amount of NAA in the brain,

$$Q_{\mathrm{NAA}} = C_B \cdot V_B \qquad [1]$$

C_B is the average NAA concentration over the entire brain tissue volume, V_B. Q_{NAA} is obtained with WBNAA to within ±6% (Benedetti et al., 2007; Gonen et al., 1998b) and V_B, from MRI-segmentation, to within ±0.5% (Clark et al., 2006; Mikheev et al., 2008). Unfortunately, the WM contributions to Q_{NAA}, cannot be separated from the GM's since,

$$Q_{\mathrm{NAA}} = C_{\mathrm{WM}} \cdot V_{\mathrm{WM}} + C_{\mathrm{GM}} \cdot V_{\mathrm{GM}} \xrightarrow{\div V_B} C_B = C_{\mathrm{WM}} \cdot F_{\mathrm{WM}} + C_{\mathrm{GM}} \cdot (1 - F_{\mathrm{WM}}), \qquad [2]$$

where V_{WM} and V_{GM} are the WM and GM volumes ($V_B=V_{WM}+V_{GM}$) and $F_{WM}=V\mathrm{WM}/V_B$ the WM fraction. Therefore, the two unknowns, C_{WM} and C_{GM}, cannot both be derived from Eq. [2].

This problem can be resolved if a second equation with the same unknowns can be obtained from another VOI, v_{VOI}, in the same brain, as shown in Fig. 1. Then, in analogy with Eq. [2],

$$q_{\mathrm{NAA}}=C_{\mathrm{WM}} \cdot v_{\mathrm{WM}}+C_{\mathrm{GM}} \cdot v_{\mathrm{GM}} \xrightarrow{\div v_{\mathrm{VOI}}} c_{\mathrm{VOI}}=C_{\mathrm{WM}} \cdot f_{\mathrm{WM}}+C_{\mathrm{GM}} \cdot (1-f_{\mathrm{WM}}), \qquad [3]$$

where q_{NAA} is the amount of NAA in v_{VOI}, v_{WM}, v_{GM} its WM and GM volumes and $f_{WM}=v_{WM}/v_{VOI}$, its WM fraction. Eq. [2] and Eq. [3] are linearly independent if in their vector form,

$$\begin{pmatrix} C_B \\ c_{\mathrm{VOI}} \end{pmatrix} = \begin{pmatrix} F_{\mathrm{WM}} & (1-F_{\mathrm{WM}}) \\ f_{\mathrm{WM}} & (1-f_{\mathrm{WM}}) \end{pmatrix} \begin{pmatrix} C_{\mathrm{WM}} \\ C_{\mathrm{GM}} \end{pmatrix}, \qquad [4]$$

the determinant of the 2×2 matrix $\neq 0$. Fortunately, due to the brain's GM and WM heterogeneity, this condition is easily met if v_b is placed judiciously to comprise different WM fractions than V_B, i.e., $F_{WM}\neq fWM$ (cf. Fig. 1 and Fig. 2). Then, Eq. [4] has a unique solution for the average global NAA concentrations of each moiety,

$$C_{\mathrm{WM}}=\frac{C_B \cdot (1-f_{\mathrm{WM}})-c_{\mathrm{VOI}} \cdot (1-F_{\mathrm{WM}})}{F_{\mathrm{WM}} \cdot (1-f_{\mathrm{WM}})-(1-F_{\mathrm{WM}}) \cdot f_{\mathrm{WM}}}; \quad C_{\mathrm{GM}}=\frac{c_{\mathrm{VOI}} \cdot F_{\mathrm{WM}}-C_B \cdot f_{\mathrm{WM}}}{F_{\mathrm{WM}} \cdot (1-f_{\mathrm{WM}})-(1-F_{\mathrm{WM}}) \cdot f_{\mathrm{WM}}} \qquad [5]$$

Materials and Methods

Human subjects

Ten healthy subjects (5 women and 5 men) mean age 28.2±5.5 (range 22 – 38) years old, with no history of neurological disorders prior to the scan and unremarkable MRI afterwards, were recruited. Their demographics are given in Table 1. All were briefed on the imaging procedure they were to undergo and gave Institutional Review Board approved written informed consent.

MRI – segmentation and volumetry

All measurements were done in a 1.5 T whole-body imager (Siemens AG, Erlangen, Germany) using its standard circularly polarized head-coil. MRI comprised T1-weighted MP-RAGE: TE/TR/TI: 7.0/14.7/300 ms; 128 slices 1.5 mm thick each, 256×256 matrix, 210×210 mm^2 field of view. Image segmentation, using the MIDAS package (De Santi et al., 2001), started by placing a "seed" region in the periventricular WM, to yield its signal intensity, I_{WM}. Following selection of all the pixels at or above $0.55I_{WM}$, a brain mask was constructed for each slice in three steps: (i) morphological erosion, (ii) recursive region growth retaining pixels connected to the "seed" region and (iii) morphological inflation to reverse the effect of erosion. An example of the result is shown in Fig. 2b. Pixels of intensity below $0.55I_{WM}$ were defined as CSF. The precision of this approach has been described previously (Rusinek and Chandra, 1993) and more recently as applied to T1-weighted imaging at 3.4% (Mikheev et al., 2008).

Next, the brain masks were truncated at the foramen magnum to incorporate the brain stem and cerebellum but not the cord. The WM mask, e.g., Fig. 2c, was constructed as the subset of all pixels with signal intensity over $0.87I_{WM}$, a value halfway between mean GM and WM for this sequence. The GM mask was the difference between the all-tissue and WM masks (cf. Fig. 2d). The same procedure was also repeated in the VOI. Finally, V_B, V_{WM}, V_{GM}, v_{VOI}, v_{WM}, and v_{GM} of Eq. [1] – Eq. [3] were obtained by multiplying the number of pixels in their masks by their volume.

MRS – Whole brain NAA (WBNAA) quantification

After shimming to a 12±2 Hz whole-head water linewidth, Q_{NAA} of Eq. [1] was obtained with non-localizing, non-echo (TE/TI/TR= 0.0/0.97/10.0 s) ^{1}H-MRS (Gonen et al., 1998b). Since the TR»T_1 and TE≈0 the sequence is insensitivity to T_1 and T_2 variations. Quantification was done against a reference 3 L sphere of 1.5×10^{-2} mole NAA in water. Subject and reference NAA peak areas, S_S and S_R, were integrated and Q_{NAA} obtained as (Soher et al., 1996),

$$Q_{NAA} = 1.5 \times 10^{-2} \cdot \frac{S_s}{S_R} \cdot \frac{V_s^{180°}}{V_R^{180°}} \text{moles.}$$

[6]

$V_R^{180°}$ and $V_s^{180°}$ are the radio-frequency voltage into 50 Ω for non-selective 1 ms 180° inversion on the reference and subject, reflecting their coil loading, *i.e.,* relative sensitivity. Note that although the peak at 2.01 ppm also comprises *N*-acetylaspartylglutamate and other acetyl-bearing species, since over 90% of it arises from the NAA (Baslow, 2003) we refer to it as such for simplicity.

Localized 3D-1H MRS quantification

A PRESS based 3D ^{1}H-MRS (TE/TR =135/1600 ms) was used to excite the image-guided 8 cm left-right (LR) ×10 cm anterior-posterior (AP) ×6 cm inferior-superior (IS) = 480 cm^3 VOI centered on the corpus callosum, as shown in Fig. 1 and Fig 2. It was partitioned with 3D hybrid of 1D-8th order Hadamard with 2D $16_{LR} \times 16_{AP}$ chemical shift imaging (CSI) into $8_{LR} \times 10_{AP} \times 8_{IS}$ = 640 voxels a nominal 0.75 cm^3 each (Gonen et al., 1998a). The protocol took under 90 minutes.

The ^{1}H-MRS signals were apodized with a 2 Hz Lorentzian, Fourier transformed along LR, AP and time, Hadamard transformed in the IS direction and automatic frequency and phase corrected in each voxel (Gonen et al., 1998a). The relative NAA amount in the jth voxel of each subject, S_j, was estimated from its peak area using parametric spectral modeling and least-squares optimization (Soher et al., 1998). All S_js were scaled into absolute, q_js, with phantom replacement, as described above (Soher et al., 1996),

$$q_j = 1.5 \times 10^{-2} \cdot \frac{S_j}{S_R} \cdot \frac{V_s^{180°}}{V_R^{180°}} \text{ moles}$$

[7]

where S_R is the average phantom voxel NAA peak area. The q_js were adjusted for relaxation time difference between the phantom *in vitro* and *in vivo*: $T_1^{vitro} = T_1^{vivo} = 1.4$ s, $T_2^{vitro}/T_2^{vivo} \approx 0.75/0.43$ s (Inglese et al., 2003),

$$q_j \approx q_j \cdot \left(1 - \frac{TE \cdot (T_2 - T_2^{vitro})}{T_2 \cdot T_2^{vitro}} \right) \cdot \frac{T_1^{vitro}}{T_1}.$$

[8]

Finally, all 640 VOI voxels' q_js, were summed to yield q_{NAA} of Eq. [3], as shown in Fig. 1. The summation *post* frequency alignment improves both the SNR and spectral resolution, as shown in Fig. 1, increasing the precision of metabolic quantification (Inglese et al., 2003). Note that this approach assumes that a single set of T_1 and T_2 values are sufficient for accurate quantification. For the former, it has been shown that for TR≈1.2·T_1 the signal, S_j in Eq. [6], varies <5% for to up to ±40% variations in T_1 (Goelman et al., 2006); and for the latter use of a single T_2 (GM and WM average) for quantification leads to S_j variations of less than 10% (Zaaraoui et al., 2007).

Statistical analyses

An exact Wilcoxon matched-pairs signed rank test was used to compare the GM and WM fractions, F_{WM} versus F_{GM} of the total brain volume and their NAA concentrations C_{WM} with

C_{GM}. An exact Wilcoxon rank sum test was used to compare these metrics between the genders. Results were declared significant if associated with a two-sided *p* value of less than 0.01.

Results

Brain volumetry

Global brain, GM and WM volumes, V_B, V_{WM}, V_{GM}, as well as their counterparts in the VOI, v_{WM}, v_{GM}, and the corresponding NAA amounts, Q_{NAA} and q_{NAA}, are given in Table 1 and their distributions shown in Fig. 3. Note that the global $F_{WM} = 39\pm3\%$ fraction (average ± standard-deviation) is indeed much different than the $f_{WM} = 70\pm4\%$ in the VOI, as required for a unique solution of Eq. [4]. Furthermore, the global WM fraction, 39±3%, in this cohort is statistically different from the GM's 60±4% with no significant sex differences (*p*>0.5), as seen in Fig. 3. These data provide 95% confidence that the gender difference in median volume is no greater than 163 cm^3 for V_{WM} and 438 cm^3 for the V_{GM}.

Brain NAA concentration

The NAA concentrations, derived from Eq. [5] using the whole brain and VOI NAA amounts and the respective tissue fractions, are given in Table 1 and their distributions shown in Fig. 3. Overall the average global WM NAA concentration, 9.5±1.0 mM, is significantly lower than the GM 14.3±1.1 mM (*p*<0.001) but with no gender differences (*p*>0.56), as seen in Fig. 3. These data provide 95% confidence that the gender difference in median NAA concentration is no greater than 2.6 mM for the C_{WM} and 2.4 mM for the G_{GM}.

Discussion

While WBNAA provides an objective specific measure of disease burden over the entire brain, it does so at the cost of complete loss of information on the regional distribution and severity of the pathological processes (Gonen et al., 1998b). Although this is nevertheless useful for monitoring several widespread whole-brain diffuse neurological disorders, *e.g.,* multiple sclerosis, HIV and trauma (Rigotti et al., 2007), other diseases involve predominantly the GM, *e.g.,* dementias, or the WM, *e.g.,* leukodystrophies (Kingsley et al., 2006; Moffett et al., 2007; Pfefferbaum et al., 1999a). Consequently, GM and WM may have different clinical relevance and prognostic value as well as response to treatment. Yet despite nearly 20 years of quantitative *in vivo* ^{1}H-MRS and extensive literature, the NAA concentration in the GM and WM of the human brain is still debated (Lopez-Villegas et al., 1996; McLean and Barker, 2006; Schuff et al., 2001). These compartmental difference motivated us to develop a method to distinguish the global NAA concentration in WM from GM, presented here. Its main departure from previous ^{1}H-MRS techniques is the trade off of regional localization for global coverage.

While the WM and GM variations in NAA concentration reported in the literature are not necessarily surprising given the myriad acquisition and data analysis approaches employed, brain regions studied, or the cohorts size, age or gender composition, this discordance makes the task of validating a new methodology more difficult. This is because absent an accepted "gold standard" for accuracy, leaves only the precision to be quantified. This is accomplished here under the operational assumptions that in young healthy adults the NAA concentrations of the WM and the GM should be *(a)* the same and *(b)* uniform. The ability of a method to reflect this amongst different individuals, given the normal variations in brain volume and its WM/GM fraction, constitutes validation and the variance in this cohort quantifies the technique's intrinsic precision.

Indeed, the leading findings are that the reproducibility, quantitatively expressed by the coefficient of variations (CV=100% ×mean/SD) is 10.5% in the WM and 7.7% in the GM. This is significantly better than the inter-subject CV≈15% for NAA in localized MRS (Chard et al., 2002; Li et al., 2002). In addition, the average NAA concentration in GM was significantly higher than in WM, in agreement with high resolution *in vitro* MRS of animal and human normal brain extracts (Florian et al., 1996; Petroff et al., 1989). Unlike *in vivo* MRS, these *in vitro* studies can monitor the metabolism of neuronal and glial cells in relative mutual isolation, yielding metabolites' concentrations from almost "pure" GM and WM. Our findings also agree with many previous *in vivo* ^{1}H-MRS reports which used multivoxel localization and rigorous segmentation (McLean and Barker, 2006).

Our study offers several improvements over the previous localized ^{1}H-MRS reports. First, the use of the WBNAA sequence eliminates the problem of bone marrow and adipose tissue lipid spectral contamination, facilitating access to the *entire* cortex. In contrast, previous studies using multislice MRS (even with surface coils that enjoyed good SNR and high special resolution) investigated GM and WM NAA levels in limited brain regions providing important but partial coverage (Lopez-Villegas et al., 1996; Noworolski et al., 1999). Second, the excellent SNR from the large volumes (whole brain and ~0.5 L VOI, see Fig. 1) improved the precision (Li et al., 2002), as reflected by the CVs in Table 1. Third, these two large volumes minimized, due to their smallest surface-to-volume ratio (SVR) the effects of GM/WM/CSF partial-volume segmentation errors at the imaging pixel level to just inter-tissue interfaces. This is compared with localized ^{1}H-MRS where this error is incurred in each and every voxel due to their (much) smaller SVR.

It is also noteworthy that the proposed approach is relatively insensitive to (unknown) T_1 and T_2 variations between the GM and WM or amongst different brain regions. Specifically, since the WBNAA method employs a very long, TR=10 s, and very short, TE =4 ms, it sustains negligible T_1 or T_2 weighting (Rigotti et al., 2007). As for the localized MRS component, recent studies have shown that normal regional NAA T_2 variations in the human brain lead to less than 10% variations is this metabolite's quantification (Zaaraoui et al., 2007). As for the dependence on tissue and regional T_1s, its has been shown that for a 90° nutation the MR signal changes by less than 5% for ±40% variation (Goelman et al., 2006). Consequently, the proposed approach is insensitive to either normal T_1 or T_2 variations.

Admittedly, the proposed approach also has several inherent limitations. First, since the concentrations are global averages, (possible) regional variations are lost or ignored even though it is documented that NAA concentrations in some GM, *e.g.,* spinal roots, medulla, pons and neurons involved in local circuits may be substantially lower than in the cortex and in motor neurons (Baslow, 2002; Moffett et al., 2007). Consequently, local changes (if they occur) are maximally diluted, *i.e.,* the approach is insensitive to focal pathology. Given the ~10% CVs, changes must exceed 20% in either compartment in order to achieve statistical significance, although such changes are often encountered in neurological disorders (Inglese et al., 2004; Rigotti et al., 2007). Second, our cohort covered only two decades (20's through 30's) of the healthy human lifespan. While this range suits the demographics of some of the common neurological disorders, such as MS, brain trauma and HIV, it does not others, *e.g.,* Alzheimer's or Parkinson's diseases. Since it is reasonable to expect that the various aging processes will affect the GM and WM of different individuals differently, it is reasonable to suspect that the precision of the approach may degrade with progressive age for elderly individuals. Finally, the small sample size (*N*=10) limits the generality of the reported findings and the observed lack of a significant gender difference, therefore, may be a reflection of its statistical power.

Conclusions

High-resolution image segmentation together with whole-brain and localized ^{1}H-MRS can exploit the structural heterogeneity of the brain to yield its average global GM and WM absolute NAA concentration. Since diffuse GM pathology is frequently the primary consequence of neurological diseases and is often the underlying cause of its cognitive sequelae; the possibility of assessing the (entire) cerebral cortex neuronal integrity is particularly attractive for monitoring neuronal changes in both natural history and experimental clinical trials.

References

Arnold DL, de Stefano N, Matthews PM, Trapp BD. N-acetylaspartate: usefulness as an indicator of viable neuronal tissue. Ann Neurol 2001;50:823. [PubMed: 11761486]discussion 824–825.

Baslow MH. Evidence supporting a role for N-acetyl-L-aspartate as a molecular water pump in myelinated neurons in the central nervous system. An analytical review. Neurochemistry International 2002;40:295–300. [PubMed: 11792458]

Baslow MH. N-acetylaspartate in the vertebrate brain: metabolism and function. Neurochem Res 2003;28:941–953. [PubMed: 12718449]

Benedetti B, Rigotti DJ, Liu S, Filippi M, Grossman RI, Gonen O. Reproducibility of the Whole-Brain N-Acetylaspartate Level across Institutions, MR Scanners, and Field Strengths. AJNR Am J Neuroradiol 2007;28:72–75. [PubMed: 17213427]

Chard DT, McLean MA, Parker GJ, MacManus DG, Miller DH. Reproducibility of in vivo metabolite quantification with proton magnetic resonance spectroscopic imaging. J Magn Reson Imaging 2002;15:219–225. [PubMed: 11836781]

Clark KA, Woods RP, Rottenberg DA, Toga AW, Mazziotta JC. Impact of acquisition protocols and processing streams on tissue segmentation of T1 weighted MR images. Neuroimage 2006;29:185–202. [PubMed: 16139526]

De Santi S, de Leon MJ, Rusinek H, Convit A, Tarshish CY, Roche A, Tsui WH, Kandil E, Boppana M, Daisley K, Wang GJ, Schlyer D, Fowler J. Hippocampal formation glucose metabolism and volume losses in MCI and AD. Neurobiol Aging 2001;22:529–539. [PubMed: 11445252]

Doyle TJ, Bedell BJ, Narayana PA. Relative concentrations of proton MR visible neurochemicals in gray and white mattter in human brain. Magn Reson Med 1995;33:755–759. [PubMed: 7651110]

Florian CL, Williams SR, Bhakoo KK, Noble MD. Regional and developmental variations in metabolite concentration in the rat brain and eye: a study using 1H NMR spectroscopy and high performance liquid chromatography. Neurochem Res 1996;21:1065–1074. [PubMed: 8897470]

Gideon P, Danielsen ER, Schneider M, Henriksen O. Short echo time proton spectroscopy of the brain in healthy volunteers using an insert gradient head coil. Magn Reson Imaging 1995;13:105–109. [PubMed: 7898269]

Goelman G, Liu S, Hess D, Gonen O. Optimizing the efficiency of high-field multivoxel spectroscopic imaging by multiplexing in space and time. Magn Reson Med 2006;56:34–40. [PubMed: 16767711]

Gonen O, Murdoch JB, Stoyanova R, Goelman G. 3D multivoxel proton spectroscopy of human brain using a hybrid of 8th-order Hadamard encoding with 2D chemical shift imaging. Magn Reson Med 1998a;39:34–40. [PubMed: 9438435]

Gonen O, Viswanathan AK, Catalaa I, Babb J, Udupa J, Grossman RI. Total brain N-acetylaspartate concentration in normal, age-grouped females: quantitation with non-echo proton NMR spectroscopy. Magn Reson Med 1998b;40:684–689. [PubMed: 9797150]

Hetherington HP, Pan JW, Mason GF, Adams D, Vaughn MJ, Twieg DB, Pohost GM. Quantitative 1H spectroscopic imaging of human brain at 4.1 T using image segmentation. Magn Reson Med 1996;36:21–29. [PubMed: 8795016]

Inglese M, Ge Y, Filippi M, Falini A, Grossman RI, Gonen O. Indirect evidence for early widespread gray matter involvement in relapsing-remitting multiple sclerosis. Neuroimage 2004;21:1825–1829. [PubMed: 15050603]

Inglese M, Li BS, Rusinek H, Babb JS, Grossman RI, Gonen O. Diffusely elevated cerebral choline and creatine in relapsing-remitting multiple sclerosis. Magn Reson Med 2003;50:190–195. [PubMed: 12815694]

Jansen JF, Backes WH, Nicolay K, Kooi ME. 1H MR spectroscopy of the brain: absolute quantification of metabolites. Radiology 2006;240:318–332. [PubMed: 16864664]

Kingsley PB, Shah TC, Woldenberg R. Identification of diffuse and focal brain lesions by clinical magnetic resonance spectroscopy. NMR Biomed 2006;19:435–462. [PubMed: 16763970]

Kreis R, Ernst T, Ross BD. Absolute quantitation of water and metabolites in the human Brain. II. Metabolite Concentrat ions. J Magn Reson. Series B 1993;102:9–19.

Li BS, Babb JS, Soher BJ, Maudsley AA, Gonen O. Reproducibility of 3D proton spectroscopy in the human brain. Magn Reson Med 2002;47:439–446. [PubMed: 11870829]

Lim KO, Spielman DM. Estimating NAA in cortical gray matter with applications for measuring changes due to aging. Magn Reson Med 1997;37:372–377. [PubMed: 9055227]

Lopez-Villegas D, Kimura H, Tunlayadechanont S, Lenkinski RE. High spatial resolution MRI and proton MRS of human frontal cortex. NMR Biomed 1996;9:297–304. [PubMed: 9134540]

McLean MA, Barker GJ. Concentrations and magnetization transfer ratios of metabolites in gray and white matter. Magn Reson Med 2006;56:1365–1370. [PubMed: 17051529]

Michaelis T, Merboldt KD, Bruhn H, Hanicke W, Frahm J. Absolute concentrations of metabolites in the adult human brain in vivo: quantification of localized proton MR spectra. Radiology 1993;187:219–227. [PubMed: 8451417]

Mikheev A, Nevsky G, Govindan S, Grossman RI, Rusinek H. Fully automatic segmentation of the brain from T1-weighted MRI using Bridge Burner algorithm. J. Magn. Reson Imag. 2008*In Press*.

Moffett JR, Ross B, Arun P, Madhavarao CN, Namboodiri AM. N-Acetylaspartate in the CNS: from neurodiagnostics to neurobiology. Prog Neurobiol 2007;81:89–131. [PubMed: 17275978]

Moonen CTW, Sobering G, van Zijl PCM, Gillen J, von Kienlin M, Bizzi A. Proton spectroscopic imaging of human brain. J. Magn. Reson 1992;98:556–575.

Narayana PA, Fotedar LK, Jackson EF, Bohan TP, Butler IJ, Wolinsky JS. Regional in vivo proton magnetic resonance spectroscopy of brain. J Magn Reson 1989;83:44–52.

Noworolski SM, Nelson SJ, Henry RG, Day MR, Wald LL, Star-Lack J, Vigneron DB. High spatial resolution 1H-MRSI and segmented MRI of cortical gray matter and subcortical white matter in three regions of the human brain. Magn Reson Med 1999;41:21–29. [PubMed: 10025607]

Petroff OA, Spencer DD, Alger JR, Prichard JW. High-field proton magnetic resonance spectroscopy of human cerebrum obtained during surgery for epilepsy. Neurology 1989;39:1197–1202. [PubMed: 2771071]

Pfefferbaum A, Adalsteinsson E, Spielman D, Sullivan EV, Lim KO. In vivo brain concentrations of N-acetyl compounds, creatine, and choline in Alzheimer disease. Arch Gen Psychiatry 1999a;56:185–192. [PubMed: 10025444]

Pfefferbaum A, Adalsteinsson E, Spielman D, Sullivan EV, Lim KO. In vivo spectroscopic quantification of the N-acetyl moiety, creatine, and choline from large volumes of brain gray and white matter: effects of normal aging. Magn Reson Med 1999b;41:276–284. [PubMed: 10080274]

Rigotti DJ, Inglese M, Gonen O. Whole-brain N-acetylaspartate as a surrogate marker of neuronal damage in diffuse neurologic disorders. AJNR Am J Neuroradiol 2007;28:1843–1849. [PubMed: 17921226]

Ross BD, Bluml S. Magnetic resonance Spectroscopy of the human brain. Anat Rec 2001;265:54–84. [PubMed: 11323770]

Rusinek H, Chandra R. Brain tissue volume measurement from magnetic resonance imaging. A phantom study. Invest Radiol 1993;28:890–895. [PubMed: 8262742]

Schuff N, Ezekiel F, Gamst AC, Amend DL, Capizzano AA, Maudsley AA, Weiner MW. Region and tissue differences of metabolites in normally aged brain using multislice 1H magnetic resonance spectroscopic imaging. Magn Reson Med 2001;45:899–907. [PubMed: 11323817]

Schuffq N, Meyerhoff DJ, Mueller S, Chao L, Sacrey DT, Laxer K, Weiner MW. N-acetylaspartate as a marker of neuronal injury in neurodegenerative disease. Adv Exp Med Biol 2006;576:241–262. [PubMed: 16802717]discussion 361–243.

Simmons ML, Frondoza CG, Coyle JT. Immunocytochemical localization of N-acetyl-aspartate with monoclonal antibodies. Neuroscience 1991;45:37–45. [PubMed: 1754068]

Soher BJ, van Zijl PC, Duyn JH, Barker PB. Quantitative proton MR spectroscopic imaging of the human brain. Magn Reson Med 1996;35:356–363. [PubMed: 8699947]

Soher BJ, Young K, Govindaraju V, Maudsley AA. Automated spectral analysis III: application to in vivo proton MR spectroscopy and spectroscopic imaging. Magn Reson Med 1998;40:822–831. [PubMed: 9840826]

Stadlbauer A, Moser E, Gruber S, Buslei R, Nimsky C, Fahlbusch R, Ganslandt O. Improved delineation of brain tumors: an automated method for segmentation based on pathologic changes of 1H-MRSI metabolites in gliomas. Neuroimage 2004;23:454–461. [PubMed: 15488395]

Tallan HH, Moore S, Stein WH. N-acetyl-L-aspartic acid in brain. J. Biol. Chem 1956;219:257–264. [PubMed: 13295277]

Tedeschi G, Righini A, Bizzi A, Barnett AS, Alger JR. Cerebral white matter in the centrum semiovale exhibits a larger N-acetyl signal than does gray matter in long echo time 1H-magnetic resonance spectroscopic imaging. Magn Reson Med 1995;33:127–133. [PubMed: 7891527]

Wang Y, Li SJ. Differentiation of metabolic concentrations between gray matter and white matter of human brain by in vivo 1H magnetic resonance spectroscopy. Magn Reson Med 1998;39:28–33. [PubMed: 9438434]

Weber-Fahr W, Ende G, Braus DF, Bachert P, Soher BJ, Henn FA, Buchel C. A fully automated method for tissue segmentation and CSF-correction of proton MRSI metabolites corroborates abnormal hippocampal NAA in schizophrenia. Neuroimage 2002;16:49–60. [PubMed: 11969317]

Zaaraoui W, Fleysher L, Fleysher R, Liu S, Soher BJ, Gonen O. Human brain-structure resolved T(2) relaxation times of proton metabolites at 3 Tesla. Magn Reson Med 2007;57:983–989. [PubMed: 17534907]
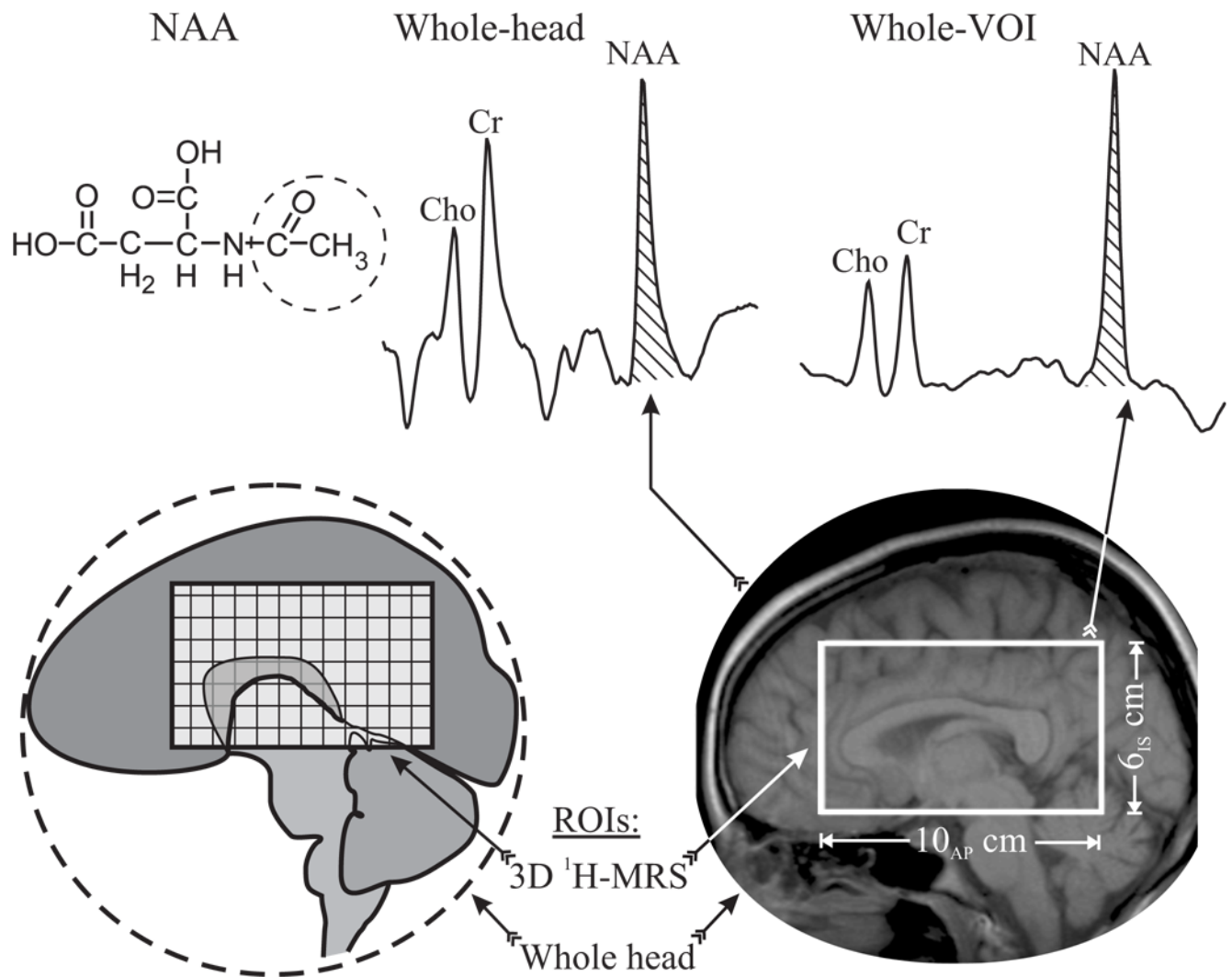
Fig. 1.
Top, left: Schematic structure of NAA with the *N*-acetyl group giving rise to the singlet at 2.01 *ppm* circled (dashed line). Center: Whole-head ^{1}H-spectrum. The NAA peak used for integration in Eq. [6] is hatched. Right: Sum of 640 aligned spectra from all 640 voxels inside the VOI with NAA area used for quantification in Eq. [7], hatched. Note the excellent SNR and spectral resolution of the sum due to its pre-alignment. Bottom: Schematic depiction of the two volumes used: Whole brain (circled region) and the $10_{AP} \times 8_{LR} \times 6_{IS}$ cm^3 PRESS VOI used to set up Eq. [2] and Eq. [3], respectively.
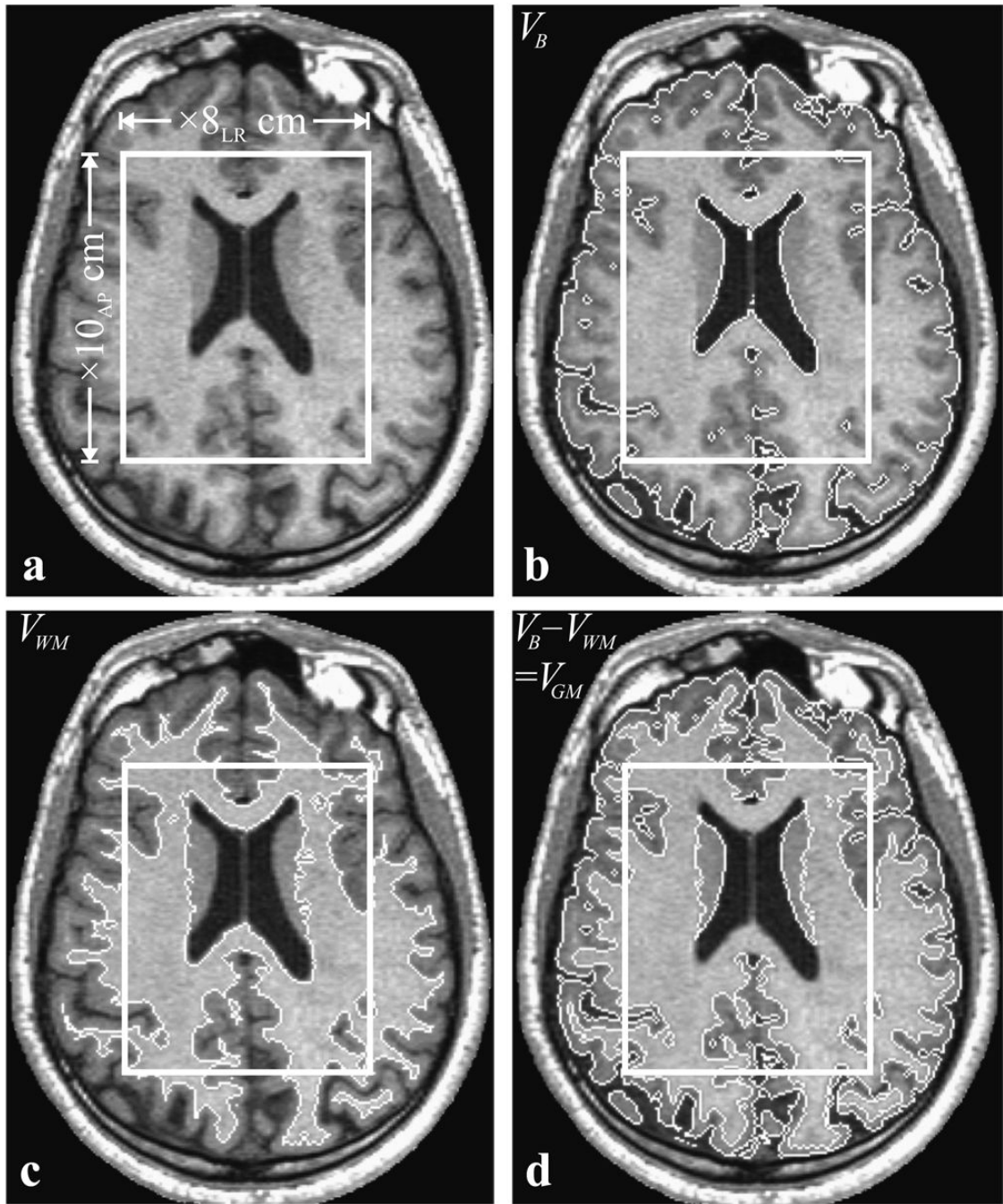
Fig. 2.
Top, left, **a**: Axial T1-weighted image showing the geometry and placement of the PRESS $10_{AP} \times 8_{LR}$ cm^2 VOI (solid frame). Top, right, **b**: Same as **a** but with the tissue mask generated by the segmentation software (white trace). Note the accurate tissue/CSF differentiation. Bottom, left, **c**: Same slice with only WM segmented and highlighted (all pixels intensities above $0.55 I_{WM}$). Bottom, right, **d**: GM mask, obtained as the **b** – **c** difference highlighted. Note the faithful tracing of the cortical ribbon and caudate at this level. All volumetry: V_B, V_{WM}, V_{GM}, v_{VOI}, v_{WM}, and v_{GM} described in the text and compiled in Table 1 were derived by counting the pixels within the corresponding masks.
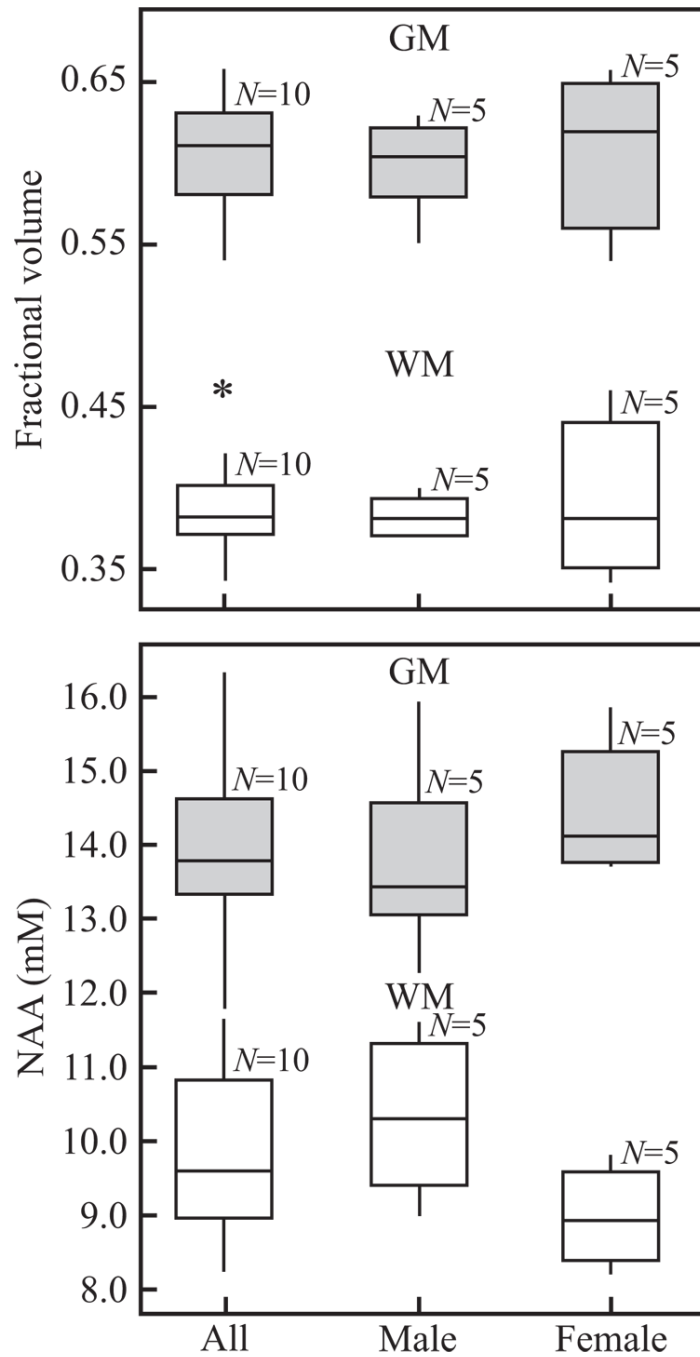
Fig. 3.
Top: Box plots displaying the 25th and 75th percentiles (box), median (line), 5th and 95th percentiles (whiskers) and outliers (*) of the GM and WM brain volume fraction distributions. Note the significant F_{WM} vs. F_{GM} difference but not between the genders. Bottom: Box plots of the average global NAA concentration in GM and WM, C_{WM}, C_{GM}, in millimoles overall and of males versus females. Note the significant concentrations difference between the compartments, but not between the genders.

Table 1

Age and gender of the cohort and the various volumetric, "V", "v" (global and VOI) and quantitative "Q" and "q" NAA metrics. The average global NAA concentration in the GM (C_{GM}) and WM (C_{GM}) compartments of each individual are estimated from Eq. [5] in the two rightmost columns (bold). Note that the average global C_{GM} is significantly higher than C_{WM} ($p<0.001$).

Subject	Age/sex[a]	$^b V_B$	$^b V_{WM}$	$^b V_{GM}$	$^b v_{VOI}$	$^b v_{WM}$	$^b v_{GM}$	$^c Q_{NAA}$	$^c q_{NAA}$	$^d C_{WM}$	$^d C_{GM}$
1	22/M	1466	557	906	457	319	124	17.8	4.8	**8.9**	**14.1**
2	22/F	1238	461	770	451	310	141	15.00	4.8	**9.0**	**14.0**
3	24/F	1098	650	410	458	309	149	13.08	4.9	**9.6**	**13.3**
4	26/M	1289	434	848	453	322	130	16.2	4.7	**8.6**	**14.6**
5	27/M	1233	521	712	447	295	146	13.5	5.0	**9.8**	**13.7**
6	27/M	1439	650	789	452	340	128	16.8	4.7	**9.4**	**13.8**
7	28/F	1331	596	735	447	319	126	15.2	5.3	**11.2**	**13.4**
8	32/F	1212	487	725	440	322	118	15.3	5.1	**10.8**	**13.5**
9	36/M	1492	532	955	453	336	116	19.6	4.6	**8.2**	**15.9**
10	38/F	1198	473	725	452	315	141	16.5	5.3	**9.8**	**16.4**
Avg±SD	28.2±5.5	1300±130	536±76	758±148	451±5	319±13	132±12	15.9±2.0	4.9±0.2	**9.5±1.0**	**14.3±1.1**

[a]Units: years

[b]Units: cm^3

[c]Units: millimoles

[d]Units: millimolar (mM).